First-Principles Study on Thermal and Electrical Transport Properties of $NbGe_2$ and $NbSi_2$: The Role of Electron–Phonon Coupling

Gui-Lin Zhu[1], Man-Yu Shang[2*], and Jing-Tao Lü[1*]

[1]*School of Physics, Institute for Quantum Science and Engineering and Wuhan National High Magnetic Field Center, Huazhong University of Science and Technology, Wuhan 430074, China*
[2]*College of Science, China Jiliang University, Hangzhou 310018, China*

(Received 14 October 2024; accepted manuscript online 15 November 2024)

We investigate coupled electron and phonon transport in NbX_2 with X=Ge, Si, where experimental evidence of strong electron–phonon coupling and hydrodynamic transport has been reported. Based on first-principles density functional theory calculations, we measured the thermal and electrical transport properties of the compounds. We found that phonon–electron scattering strongly affects phonon thermal conductivity ($\kappa_{\rm ph}$) and leads to a weak temperature dependence of $\kappa_{\rm ph}$ instead of a normal inverse temperature dependence when anharmonic three-phonon scattering dominates. In addition, $\kappa_{\rm ph}$ contributes to a quarter of the total thermal conductivity, which differs from typical metals in which the total thermal conductivity is predominantly derived from electrons. In contrast to previous numerical research, our electrical resistivity results agree well with the experimental measurements. The anisotropic properties of the transport coefficients are attributed to the electron–phonon dispersion relation. In addition, we found a negligible effect of electron–phonon drag on the transport properties, contrary to the expectation from a strongly coupled electron–phonon fluid.

DOI: 10.1088/0256-307X/41/12/126301

1. Introduction. The transport properties of solids are important for understanding their fundamental physical properties and potential device applications. Thermal transport exhibits a variety of phenomena, such as the phonon focusing effect and interlayer van der Waals modulation.[1,2] For a very long time, the limited lattice thermal conductivity was attributed to the phonon–phonon (ph–ph) anharmonic interaction (PPI), and the phonon–electron (ph–e) interaction (PEI) was thought to contribute to lattice thermal conductivity only at low temperatures.[3–5] This conclusion was followed until the discovery that the lattice thermal conductivity could be reduced by 45% in heavily doped silicon at room temperature by adjusting the carrier concentration.[6] Since then, many studies have revealed the significant effects of PEI on the reduction of lattice thermal conductivity in metals and thermoelectric materials.[7–12]

However, these results were based on Bloch's assumption that the phonon (electron) Boltzmann transport equation (BTE) could be solved when electrons (phonons) remain in equilibrium. Because electrons and phonons are coupled, a deviation from the equilibrium of one species drags the other out of equilibrium. The mutual drag effect was first formulated by L. E. Gurevich in 1946 and systematically reviewed by Y. G. Gurevich in 1989.[13] Recently, Protik *et al.* presented a solution for fully coupled electron–phonon (e–ph) BTEs, and they found that phonon drags significantly affect mobility, whereas electron drag has only a small effect on lattice thermal conductivity in n-doped gallium arsenide.[14]

Experimental research has revealed an enhanced quasiparticle mass, anomalous temperature dependence of the phonon linewidth, and smaller electrical resistivity than theoretical calculations in $NbGe_2$.[15,16] These results indicate a phonon-mediated hydrodynamic flow in $NbGe_2$ due to the frequent exchange of crystal momenta between electrons and phonons. If this is the case, the mutual drag between electrons and phonons should be strong, which may have a signature in the transport coefficients. This prompts us to quantitatively investigate the extent to which the drag effect affects the transport properties of phonons and electrons in this material, which requires a solution of coupled electron and phonon BTEs.[17]

In this study, we illustrate that ph–e scattering rates exceed anharmonic ph–ph scattering rates over a wide range of frequencies, resulting in a significant reduction in lattice thermal conductivity. Considering electron thermal conductivity, we found that the total thermal conductivity was significantly influenced by e–ph interactions (EPIs). In contrast, the drag effect has an impact on the transport properties, which is two orders of magnitude smaller than the original results under Bloch's assumption, making it negligible.

2. Methods. The BTEs for phonons (pBTE) and electrons (eBTE) are expressed as follows:

$$\begin{aligned}&\frac{\partial n_{s\boldsymbol{q}}}{\partial t}+\boldsymbol{v}_{s\boldsymbol{q}}\cdot\nabla_{\boldsymbol{r}}n_{s\boldsymbol{q}}=\left(\frac{\partial n_{s\boldsymbol{q}}}{\partial t}\right)_{\rm coll},\\&\frac{\partial f_{m\boldsymbol{k}}}{\partial t}+\boldsymbol{v}_{m\boldsymbol{k}}\cdot\nabla_{\boldsymbol{r}}f_{m\boldsymbol{k}}+\boldsymbol{F}_{m\boldsymbol{k}}\cdot\nabla_{\boldsymbol{k}}f_{m\boldsymbol{k}}=\left(\frac{\partial f_{m\boldsymbol{k}}}{\partial t}\right)_{\rm coll},\end{aligned}\quad(1)$$

*Corresponding author. Email: shmy25@cjlu.edu.cn; jtlu@hust.edu.cn
© 2024 Chinese Physical Society and IOP Publishing Ltd

where $n_{s\boldsymbol{q}}/f_{m\boldsymbol{k}}$ denotes the distribution function of the phonon/electron system, $\boldsymbol{v}_{s\boldsymbol{q}}/\boldsymbol{v}_{m\boldsymbol{k}}$ denotes the group velocity, and $\boldsymbol{F}_{m\boldsymbol{k}}$ denotes the force exerted by an external field on the electrons. The subscripts (s, $\boldsymbol{q}$) and (m, $\boldsymbol{k}$) are the band index and wave vector for the phonon and electron, respectively. When the external field (electric or magnetic) alters the drift term in the eBTE, the collision term also changes accordingly. Due to EPIs, the collision term in pBTE also changes. The external field drives both systems out of equilibrium. Therefore, the transport of phonons and electrons is coupled.

According to the derivation by Protik *et al.*,[17] phonon thermal conductivity is given by

$$\kappa_{\mathrm{ph}} = \frac{1}{Vk_{\mathrm{B}}T}\sum_{s\boldsymbol{q}} \hbar\omega_{s\boldsymbol{q}} n^0_{s\boldsymbol{q}}(1+n^0_{s\boldsymbol{q}})\boldsymbol{v}_{s\boldsymbol{q}} \otimes \boldsymbol{F}_{s\boldsymbol{q}}, \tag{2}$$

where $\boldsymbol{v}_{s\boldsymbol{q}}$ denotes the phonon group velocity and $\boldsymbol{F}_{s\boldsymbol{q}}$ denotes the phonon response function due to the applied ∇T field, which is given by

$$\boldsymbol{F}_{s\boldsymbol{q}} = \boldsymbol{F}^0_{s\boldsymbol{q}} + \Delta\boldsymbol{F}^S_{s\boldsymbol{q}}[\boldsymbol{F}_{s\boldsymbol{q}}] + \Delta\boldsymbol{F}^{\mathrm{D}}_{s\boldsymbol{q}}[\boldsymbol{I}_{m\boldsymbol{k}}], \tag{3}$$

where the terms with the superscript 0, S, and D represent the relaxation time approximation (RTA), self, and drag terms, respectively. Here, $\boldsymbol{I}_{m\boldsymbol{k}}$ denotes the electron response function resulting from the applied ∇T field. The specific expressions of $\boldsymbol{F}^0_{s\boldsymbol{q}}$, $\Delta\boldsymbol{F}^S_{s\boldsymbol{q}}$, $\Delta\boldsymbol{F}^{\mathrm{D}}_{s\boldsymbol{q}}$, and $\boldsymbol{I}_{m\boldsymbol{k}}$ can be found in Ref. [17]. By retaining different levels of solutions of $\boldsymbol{F}_{s\boldsymbol{q}}$, we obtain the phonon thermal conductivity under RTA (κ^0_{ph}) and include the drag effects ($\kappa^{\mathrm{D}}_{\mathrm{ph}}$). Similarly, for electrons, the electrical resistivity is given by

$$\frac{1}{\rho} = \frac{d_s e}{Vk_{\mathrm{B}}T}\sum_{m\boldsymbol{k}} f^0_{m\boldsymbol{k}}(1-f^0_{m\boldsymbol{k}})\boldsymbol{v}_{m\boldsymbol{k}} \otimes \boldsymbol{J}_{m\boldsymbol{k}}, \tag{4}$$

where $\boldsymbol{J}_{m\boldsymbol{k}}$ denotes the electron response function resulting from the applied $\boldsymbol{E}$ field. By retaining different levels of solutions of $\boldsymbol{J}_{m\boldsymbol{k}}$, we obtain the electrical resistivity under RTA (ρ^0) and include the drag effects (ρ^{D}).

The mode-resolved phonon thermal conductivity is the result prior to summation in Eq. (2) with

$$\kappa^0_{s\boldsymbol{q}} = \frac{1}{Vk_{\mathrm{B}}T}\hbar\omega_{s\boldsymbol{q}} n^0_{s\boldsymbol{q}}(1+n^0_{s\boldsymbol{q}})\boldsymbol{v}_{s\boldsymbol{q}} \otimes \boldsymbol{F}^0_{s\boldsymbol{q}}, \tag{5}$$

$$\kappa^{\mathrm{D}}_{s\boldsymbol{q}} = \frac{1}{Vk_{\mathrm{B}}T}\hbar\omega_{s\boldsymbol{q}} n^0_{s\boldsymbol{q}}(1+n^0_{s\boldsymbol{q}})\boldsymbol{v}_{s\boldsymbol{q}} \otimes \boldsymbol{F}^{\mathrm{D}}_{s\boldsymbol{q}}, \tag{6}$$

where $\kappa^0_{s\boldsymbol{q}}$ and $\kappa^{\mathrm{D}}_{s\boldsymbol{q}}$ are the results obtained under the RTA and drag effects, respectively.

Table 1. Quantities, explanation, and corresponding graph.

Quantities	Explanation	Graph
$\kappa^{\mathrm{PP}}_{\mathrm{ph}}$	RTA phonon thermal conductivity include PPI only	Fig. 2
κ^0_{ph}	RTA phonon thermal conductivity include PPI and EPI	Fig. 2 and Fig. 3
$\kappa^{\mathrm{D}}_{\mathrm{ph}}$	Electron-dragged phonon thermal conductivity	Fig. 3
$\kappa^0_{s\boldsymbol{q}}$	RTA mode-resolved phonon thermal conductivity including PPI and EPI	Fig. 3
$\kappa^{\mathrm{D}}_{s\boldsymbol{q}}$	Electron-dragged mode-resolved phonon thermal conductivity	Fig. 3
ρ^0	RTA electrical resistivity	Fig. 4
ρ^{D}	Phonon-dragged electrical resistivity	Fig. 4
$\kappa^{\mathrm{D}}_{\mathrm{e}}$	Phonon-dragged electron thermal conductivity	Fig. 5
$\kappa^{\mathrm{D}}_{\mathrm{tot}}$	Electron-dragged total thermal conductivity	Fig. 5

The computed codes and the corresponding graph of the above quantities are summarized in Table 1. For the numerical calculations, we calculated the anharmonic ph–ph scattering rates using the Vienna Ab initio Simulation Package coupled with the Phono3py Package and the ShengBTE Package.[18–21] The projector augmented wave approach and the Perdew–Burke–Ernzerhof exchange-correlation functional were used.[22,23] We employed a $2\times2\times2$ supercell and 5.0 Å cutoff pair-distance to obtain the third-order force constants. The $2\times2\times2$ supercell was sufficient for calculating the thermal conductivity (Fig. S1 in Supplemental Material). A cutoff energy of 400 (450) eV was adopted, and the Brillouin zone was sampled with a $3\times3\times2$ Γ-centered k-point grid for $NbGe_2$ ($NbSi_2$). For the e–ph scattering rate calculation, we used the Quantum ESPRESSO and electron–phonon Wannier packages.[24,25] We used fully relativistic norm-conserving pseudopotentials and the PBEsol exchange-correlation functional, and the cutoff energy was set to 82 Ry, with Marzari–Vanderbilt ("cold") smearing with 0.002 Ry.[26–28] An initial coarse $4\times4\times3$ q and $10\times10\times8$ k points were used to calculate the phonon and electron states and e–ph coupling matrix elements using density functional perturbation theory.[29] We then used 66 maximally localized Wannier functions to fit the density functional theory (DFT) electron states[30,31] (Fig. S2). After the convergence tests (Fig. S3), we adopted a dense mesh of $50\times50\times40$ k and $25\times25\times20$ q points to obtain accurate phonon and electron scattering rates in the temperature range 50–600 K. Then, the lattice thermal conductivity, along with ph–ph and ph–e scattering rates, was calculated using the Phono3py program. Finally, we calculated the phonon (or electron) transport properties, along with the electron (or phonon) drag effect, using the epiboly program,[17] where $28\times28\times28$ k and $14\times14\times14$ q points were used (Fig. S4).

3. Results and Discussions.

3.1. Lattice Structure, Electronic and Phononic Band. The crystal structures of $NbGe_2$ and $NbSi_2$ belong to the hexagonal C40 structural group with two different types of chirality. The right- and left-handed structures crystallize in the space group $P6_222$ (No. 180) and $P6_422$ (No. 181), respectively.[32,33] For comparison with the experimental results, we focus on the right-handed struc-

tures in this study. As shown in Fig. 1(a), the chirality originates from the presence of a double helix Ge/Si atom along the c axis. The optimized lattice parameters ($a = b = 5.009$ Å, $c = 6.837$ Å for $NbGe_2$ and $a = b = 4.815$ Å, $c = 6.622$ Å for $NbSi_2$) are consistent with previous first-principles and experimental studies.[16,32–34] Each Nb atom exhibits dodecahedral coordination with the 10 surrounding Ge/Si atoms. The bond lengths of NbGe and NbSi are 2.705–2.913 Å and 2.625–2.841 Å, respectively. According to previous results, short metallic bond lengths may be beneficial for phonon-dragged electron hydrodynamics.[16,35]

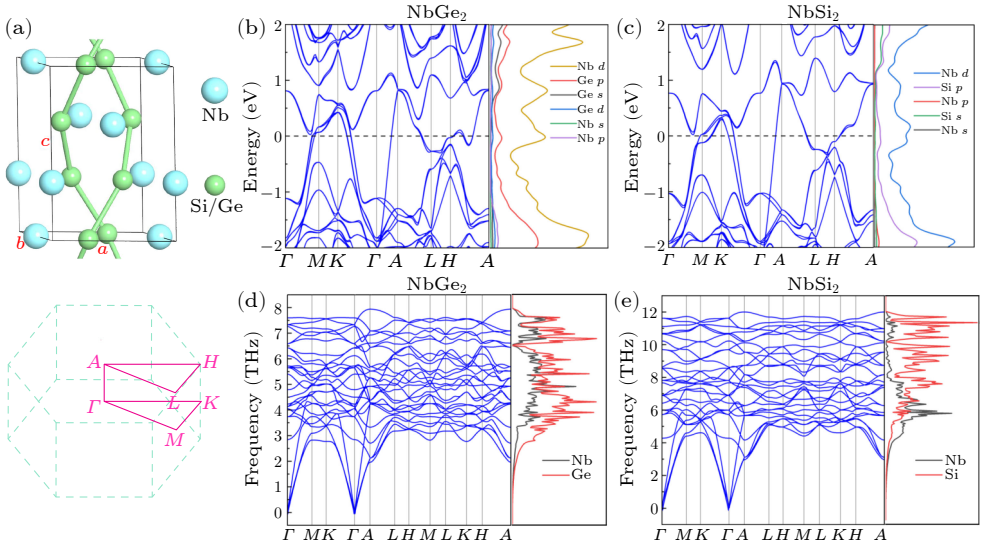

Fig. 1. (a) Crystal structure and first Brillouin zone of right-handed NbX_2 (X=Ge and Si). The double helix has been shifted into the center of the lattice for clarity. [(b), (c)] Electronic and [(d), (e)] phononic band structures of $NbGe_2$ and $NbSi_2$. The Fermi level is set to zero. The side panels on the right show the orbital or atom-resolved density of states.

Figures 1(b) and 1(c) show the electronic band structures for $NbGe_2$ and $NbSi_2$ at a Fermi level of ±2 eV. The band structures of the two compounds are similar. They are metallic and exhibit band splitting near the Fermi energy due to strong spin-orbit coupling. The phonon dispersion is shown in Figs. 1(d) and 1(e). All phonon branches consist of 3 acoustic branches and 24 optical branches. The highest optical phonon frequency of $NbGe_2$ ($\sim$ 8 THz) is smaller than that of $NbSi_2$ ($\sim$ 12 THz) because of the light atomic mass of the Si atom. The electron and phonon dispersion results agree with those reported in previous research[15] and obtained by different DFT programs (Fig. S2).

3.2. Phonon Thermal Conductivity. In metals, electrons are typically considered major heat carriers, and the contribution of phonons is negligible.[36–38] However, there are also some exceptions, such as metallic tungsten carbide, group-V transition metal carbides, and elemental W.[39–41] Here, we first explore the phonon transport properties of $NbGe_2$ and $NbSi_2$ and then calculate their electron thermal conductivities. Anharmonic three-phonon (3ph) scattering and ph–e scattering were considered in our calculations, whereas other scattering processes, including phonon-isotope scattering and four-phonon scattering, were ignored. Figures 2(a) and 2(b) illustrate the temperature-dependent phonon thermal conductivity of $NbGe_2$ and $NbSi_2$ under RTA that includes both PEI and PPI (κ_{ph}^{0}) and RTA that includes only PPI (κ_{ph}^{PP}). The results obtained along b are the same as those obtained along a and are not shown. The temperature dependence of κ_{ph}^{PP} approximately follows the T^{-1} relation in the high-temperature regime. A significant reduction in the low-temperature regime was observed after including ph–e scattering. In addition, we plotted the phonon scattering rates contributed by 3ph and ph–e scattering at 300 K (Fig. S5), and the ph–e and 3ph scattering rates were comparable. In particular, for $NbGe_2$, the ph–e scattering rates of the low-frequency acoustic phonon modes are one order of magnitude larger than the 3ph scattering rates, resulting in a more obvious decrease in phonon thermal conductivity. Thus, phonon scattering by electrons is not negligible and plays an important role in modifying the temperature dependence of phonon thermal conductivity.[8,42–45]

In addition, the phonon thermal conductivity of both compounds is anisotropic. The κ_{ph} in the c direction is larger than that in the a direction. The reason for this anisotropy is provided in the final section of this paper. Conversely, the κ_{ph} of $NbSi_2$ is larger than that of $NbGe_2$ over the entire temperature range. Taking 300 K as an example, the smaller average lifetime and group velocity of acoustic phonons (Table S1) may explain the smaller κ_{ph} of $NbGe_2$ (Table S1).

Next, to investigate the impact of the drag effect on the phonon transport properties, the epiboly code was used to iteratively solve the coupled e–ph BTEs. As shown in Figs. 3(a) and 3(b), the drag effect on the phonon thermal conductivities of both materials is minimal, even at low

temperatures. Therefore, we plotted the mode-resolved phonon thermal conductivity of $NbGe_2$ under different approximations to analyze the specific influence of the drag effect on each phonon mode [Figs. 3(c) and 3(d)]. In the RTA solution, the phonon thermal conductivity was primarily contributed by the low-frequency phonon modes, which is consistent with the common understanding. In the drag solution, the added in-scattering term opened the channel for the exchange of momentum between other phonons, and the drag term enabled the phonons to exchange momentum with electrons. The contribution to thermal conductivity was not always positive compared with that of the RTA solution. The low-frequency phonons were more sensitive to drag effects than the high-frequency phonons. This is because the phonon modes did not exhibit significant selectivity in response to the electron drag effect, and the lower-frequency modes contributed more to thermal conductivity due to their higher occupation number and heat capacity. Many modes exhibit a decrease in the contribution. Overall, the drag effect impacts thermal conductivity that is numerically two orders of magnitude smaller; thus, it can be neglected.

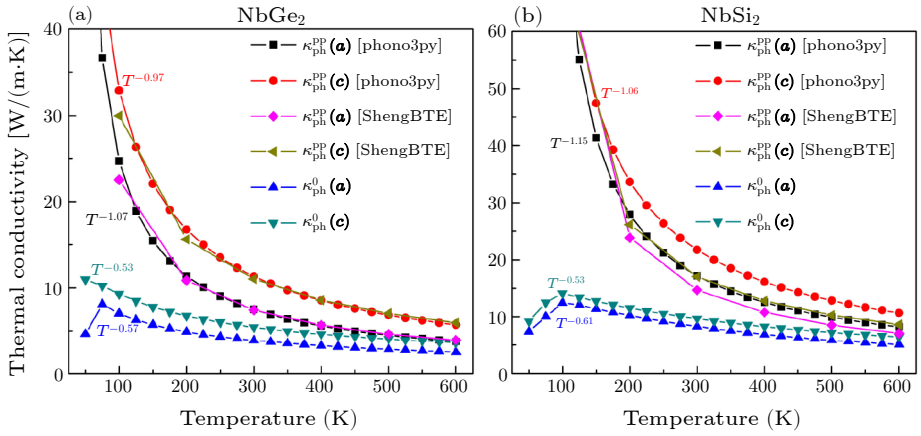

Fig. 2. Phonon thermal conductivity as a function of temperature for (a) $NbGe_2$ and (b) $NbSi_2$.

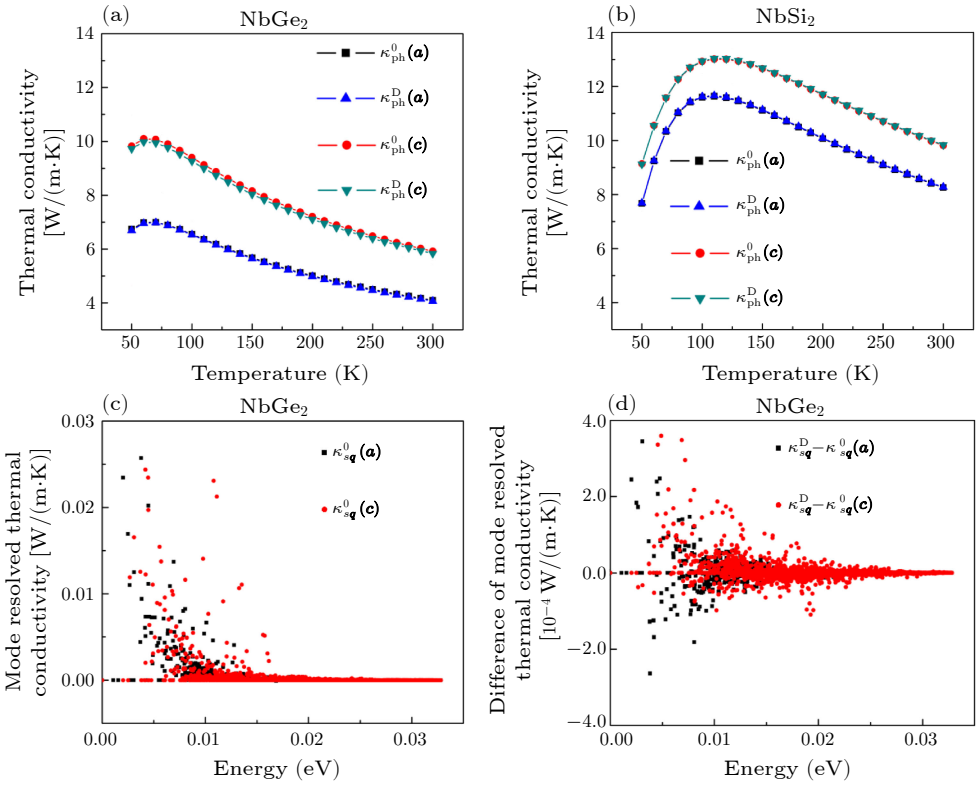

Fig. 3. Temperature dependence of lattice thermal conductivity of (a) $NbGe_2$ and (b) $NbSi_2$ computed from RTA and self-consistent solutions of BTEs, labeled as κ^0_{ph} and κ^D_{ph}, respectively. (c) Lattice thermal conductivity contributed by each phonon mode in RTA solution for $NbGe_2$ at 50 K. (d) Difference in mode-resolved thermal conductivity between drag and RTA solutions for $NbGe_2$ at 50 K.

3.3. Electrical Resistivity and Electron Thermal Conductivity. Recent work has revealed a discrepancy between the theoretically calculated and experimentally measured resistivity values in $NbGe_2$, and the plausible source is the recycling of momentum from phonons to electrons (phonon drag).[15,16] Thus, we evaluated the effect of phonon drag on electrical resistivity and thermal conductivity. As shown in Fig. 4, the electrical resistivity of both materials exhibits varying degrees of anisotropy, with higher resistance in the a (in-plane) direction than in the c (out-of-plane) direction. The in-plane resistivity was 78.3 (∼50,[16,46] ∼60,[47] 67,[48] and ∼80[34]) μΩ·cm for $NbGe_2$ and 29.7 (∼20[49]) μΩ·cm for $NbSi_2$ at 300 K. Similar anisotropic behavior was observed for phonon conductivity, as previously demonstrated. We attribute this to the anisotropic phonon and electron band structures and provide detailed analysis at the end of this paper.

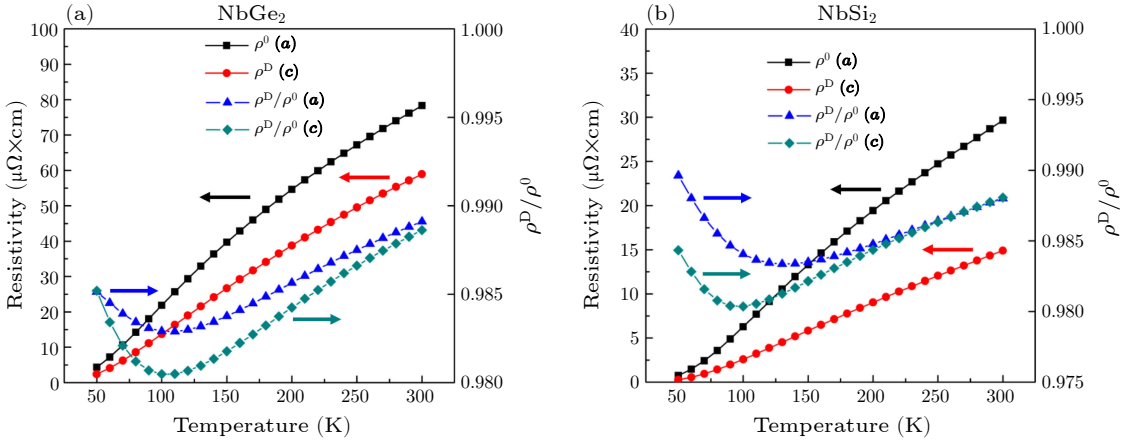

Fig. 4. Temperature dependence of resistivity with drag effect (ρ^{D}) and ratio of resistivity with drag effect to that with RTA ($\rho^{\mathrm{D}}/\rho^{0}$) for (a) $NbGe_2$ and (b) $NbSi_2$. The arrows indicate whether the corresponding curve is associated with the left or right y-axis.

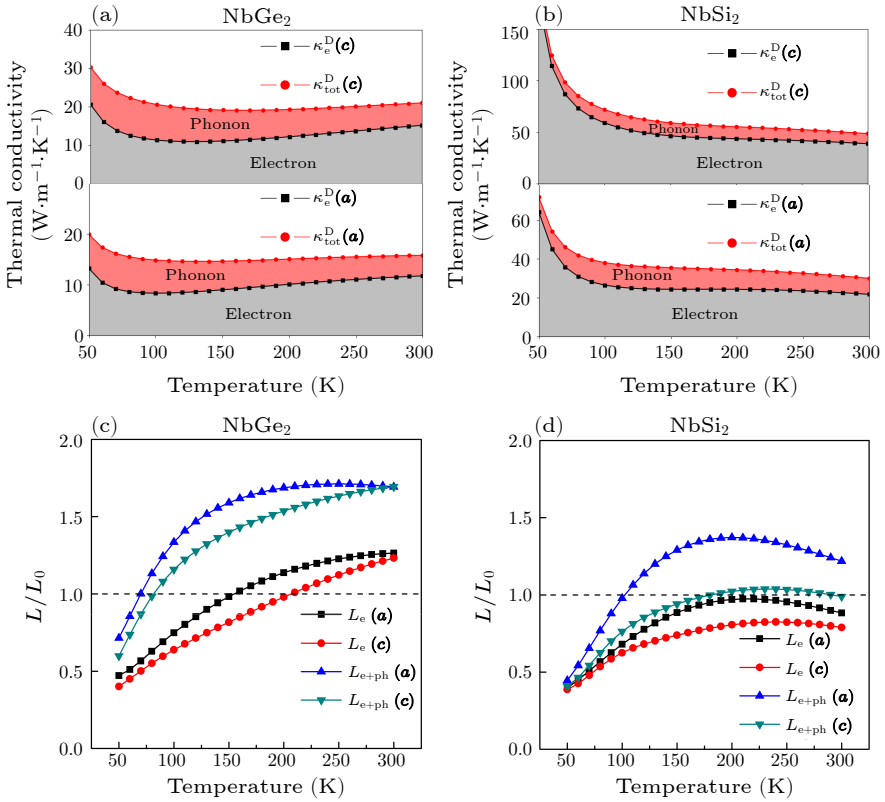

Fig. 5. (a) and (b) Temperature dependence of electron and total thermal conductivity for $NbGe_2$ and $NbSi_2$. (c) and (d) Temperature dependence of the renormalized Lorenz number with $L_{\mathrm{e}} = \kappa_{\mathrm{e}}/T\sigma$, $L = \kappa_{\mathrm{tot}}/T\sigma$, and $L_0 = \pi^2 k_{\mathrm{B}}^2/3e^2$.

In addition, the drag effect on electrical resistivity is weak in both $NbGe_2$ and $NbSi_2$ (approximately 2% decreases at most around 100 K). The parabolic trends originated from the absence of phonon excitation at low temperatures and nondominant EPIs at higher temperatures. Notably, the reported anomalously large electrical resistivity along a direction in $NbGe_2$ was not observed in this study.[12] The ∼10-THz phonon linewidth of the optical modes near Γ for $NbGe_2$ in previous research, which exceeds the phonon frequency, is absent in our results.

In terms of electron thermal conductivity, the drag effect was also negligible. Thus, we only plot the results with the drag effect (κ_e^D) and the total thermal conductivity (κ_{tot}^D) with both the electron and phonon contribution in Figs. 5(a) and 5(b). The κ_e^D of $NbSi_2$ is greater than that of $NbGe_2$ over the entire temperature range. At 300 K, the κ_e^D values of $NbGe_2$ are 11.8 W/(m·K) along a and 15.2 W/(m·K) along c, and the corresponding κ_e^D values of $NbSi_2$ are 21.8 and 38.7 W/(m·K), respectively. Compared with normal metals, the relatively small electronic thermal conductivities of $NbGe_2$ and $NbSi_2$ lead to the non-negligible phonon component. The ratios of the phonon component to the total thermal conductivity are 26%–28% for $NbGe_2$ and 20%–28% for $NbSi_2$ at 300 K. The c-direction thermal conductivities of $NbGe_2$ [21.0 W/(m·K)] and $NbSi_2$ [48.5 W/(m·K)] agree reasonably well with the experimental results [31 W/(m·K) for $NbGe_2$ and 42 W/(m·K) for $NbSi_2$].[48] Based on these results, the obtained Lorenz numbers for $NbGe_2$ and $NbSi_2$ are shown in Figs. 5(c) and 5(d), respectively. A deviation from the standard value was observed for both materials.

Finally, we discuss the anisotropic transport properties of both materials. The thermal and electrical conductivity along the c direction is larger than that along b/a. This transport anisotropy already appears in the RTA. Thus, we limit our discussion within the RTA. Electrical conductivity depends on the group velocity and relaxation time of quasiparticles, and thermal conductivity depends on specific heat capacity. The quasiparticle group velocity and specific heat capacity are primarily determined by the dispersion relation in the RTA, whereas the relaxation time is influenced by different scattering processes. A comparison of the thermal and electrical conductivities under constant RTA (Fig. S4) indicates that the dispersion relation is the primary reason for the anisotropy. This is also reflected in Fig. 6 in which the squares of the modal group velocities along the a and c directions are plotted. Both electrons and phonons have a broader and larger average velocity along c, resulting in higher conductivity (smaller resistivity).

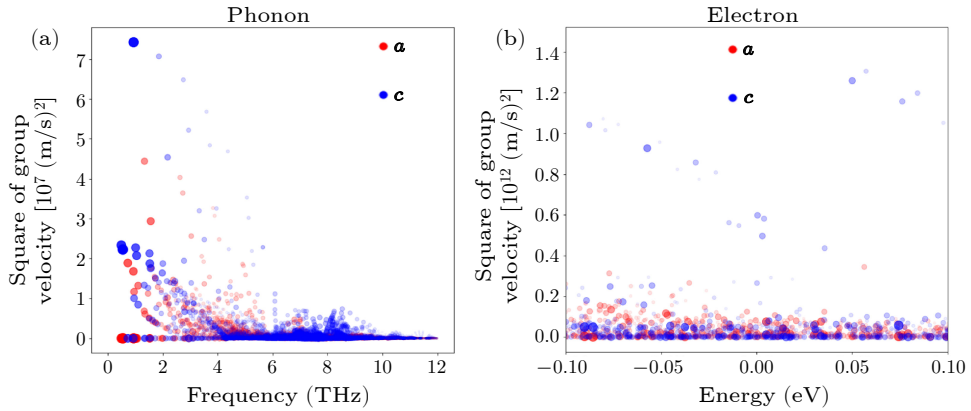

Fig. 6. Square of (a) phonon and (b) electron group velocity in a (red) and c (blue) directions for $NbGe_2$. The size and transparency of the points represent the magnitude of relaxation time. Smaller, transparent dots represent shorter relaxation times and less contribution to conductivity. The Fermi energy is set to 0 in (b).

4. Conclusions. In summary, we have presented a first-principles study on the electrical and thermal transport properties of $NbSi_2$ and $NbGe_2$ considering the e–ph, ph–e, and anharmonic 3ph scattering processes. The electrical and thermal transport coefficients show similar anisotropy with higher conductivity along the c direction, originating from the electron and phonon band structures of $NbSi_2$ and $NbGe_2$. We found that approximately one-quarter of the total thermal conductivity is contributed by phonons with weak temperature dependence, indicating the important role played by ph–e scattering. The obtained electrical conductivity/resistivity reasonably agrees with the reported experimental values but deviates from previous numerical calculations. However, by solving the coupled electron and phonon BTEs self-consistently, we found a negligible effect of the e–ph drag on the transport properties. Considering the experimentally observed electron mass enhancement and temperature-dependent Raman signals, which are not captured by standard DFT calculations, we speculate that more advanced electronic structure calculations are required to fully understand the transport properties.

Acknowledgements. The authors are grateful for the valuable communication with N. H. Protik. This work was supported in part by the National Natural Science Foundation of China (Grant No. 22273029) and the Natural Science Foundation of Zhejiang Province, China (Grant No. 20230021).

References

[1] Jiang J H, Lu S, and Chen J 2023 *Chin. Phys. Lett.* **40** 096301
[2] Ren W, Lu S, Yu C, He J, Zhang Z, Chen J, and Zhang G 2023 *Appl. Phys. Rev.* **10** 041404
[3] Makinson R E B 1938 *Math. Proc. Cambridge Philos. Soc.* **34** 474
[4] Klemens P 1954 *Australian Journal of Physics* **7** 57
[5] Tan R, Ouyang Y, Li L, Zeng Y, Tang Z, Zhang Z, and Chen J 2024 *J. Phys. D* **57** 505305
[6] Liao B, Qiu B, Zhou J, Huberman S, Esfarjani K, and Chen G 2015 *Phys. Rev. Lett.* **114** 115901
[7] Zhu Z, Xi J, and Yang J 2022 *J. Mater. Chem. A* **10** 13484
[8] Wang A, Li S, Zhang X, and Bao H 2022 *Phys. Rev. Mater.* **6** 014009
[9] Yan Y, Li N, Wang G, Xiong Q, Fan L, Jiang P, Lu X, Wang G, and Zhou X 2022 *Materials Today Physics* **22** 100590
[10] Huang Y, Zhou J, Wang G, and Sun Z 2019 *J. Am. Chem. Soc.* **141** 8503
[11] Li S, Wang A, Hu Y, Gu X, Tong Z, and Bao H 2020 *Materials Today Physics* **15** 100256
[12] Tao Y, Pan Z, Ruch T, Zhan X, Chen Y, Zhang S X, and Li D 2021 *Materials Today Physics* **21** 100517
[13] Gurevich Y G and Mashkevich O L 1989 *Physics Reports* **181** 327
[14] Protik N H and Broido D A 2020 *Phys. Rev. B* **101** 075202
[15] Garcia C A C, Nenno D M, Varnavides G, and Narang P 2021 *Phys. Rev. Mater.* **5** L091202
[16] Yang H Y, Yao X H, Plisson V, Mozaffari S, Scheifers J P, Savvidou A F, Choi E S, McCandless G T, Padlewski M F, Putzke C *et al.* 2021 *Nat. Commun.* **12** 5292
[17] Protik N H, Li C, Pruneda M, Broido D, and Ordejón P 2022 *npj Computational Materials* **8** 28
[18] Kresse G and Hafner J 1993 *Phys. Rev. B* **48** 13115
[19] Togo A, Chaput L, and Tanaka I 2015 *Phys. Rev. B* **91** 094306
[20] Togo A, Chaput L, Tadano T, and Tanaka I 2023 *J. Phys.: Condens. Matter* **35** 353001
[21] Li W, Carrete J, Katcho N A, and Mingo N 2014 *Computer Physics Communications* **185** 1747
[22] Blöchl P E 1994 *Phys. Rev. B* **50** 17953
[23] Perdew J P, Burke K, and Ernzerhof M 1996 *Phys. Rev. Lett.* **77** 3865
[24] Giannozzi P, Baroni S, Bonini N, Calandra M, Car R, Cavazzoni C, Ceresoli D, Chiarotti G L, Cococcioni M, Dabo I, Corso A D, de Gironcoli S, Fabris S, Fratesi G, Gebauer R, Gerstmann U, Gougoussis C, Kokalj A, Lazzeri M, Martin-Samos L, Marzari N, Mauri F, Mazzarello R, Paolini S, Pasquarello A, Paulatto L, Sbraccia C, Scandolo S, Sclauzero G, Seitsonen A P, Smogunov A, Umari P, and Wentzcovitch R M 2009 *J. Phys.: Condens. Matterr* **21** 395502
[25] Poncé S, Margine E R, Verdi C, and Giustino F 2016 *Computer Physics Communications* **209** 116
[26] Hamann D R 2013 *Phys. Rev. B* **88** 085117
[27] Perdew J P, Ruzsinszky A, Csonka G I, Vydrov O A, Scuseria G E, Constantin L A, Zhou X, and Burke K 2008 *Phys. Rev. Lett.* **100** 136406
[28] Marzari N, Vanderbilt D, De Vita A, and Payne M C 1999 *Phys. Rev. Lett.* **82** 3296
[29] Baroni S, de Gironcoli S, Dal Corso A, and Giannozzi P 2001 *Rev. Mod. Phys.* **73** 515
[30] Marzari N and Vanderbilt D 1997 *Phys. Rev. B* **56** 12847
[31] Souza I, Marzari N, and Vanderbilt D 2001 *Phys. Rev. B* **65** 035109
[32] Ertürk E and Gürel T 2018 *Physica B: Condensed Matter* **537** 188
[33] Sakamoto H, Fujii A, Tanaka K, and Inui H 2005 *Acta Materialia* **53** 41
[34] Lv B, Li M, Chen J, Yang Y, Wu S, Qiao L, Guan F, Xing H, Tao Q, Cao G H, and Xu Z A 2020 *Phys. Rev. B* **102** 064507
[35] Moll P J W, Kushwaha P, Nandi N, Schmidt B, and Mackenzie A P 2016 *Science* **351** 1061
[36] Ziman J M 2001 *Electrons and phonons: the theory of transport phenomena in solids* (Oxford university press)
[37] Li S, Yang X, Hou J, and Du W 2020 *Journal of Magnesium and Alloys* **8** 78
[38] Burger N, Laachachi A, Ferriol M, Lutz M, Toniazzo V, and Ruch D 2016 *Progress in Polymer Science* **61** 1
[39] Kundu A, Ma J, Carrete J, Madsen G K H, and Li W 2020 *Materials Today Physics* **13** 100214
[40] Li C, Ravichandran N K, Lindsay L, and Broido D 2018 *Phys. Rev. Lett.* **121** 175901
[41] Chen Y, Ma J, and Li W 2019 *Phys. Rev. B* **99** 020305
[42] Zhou Z, Yang X, Fu H, Wang R, Lu X, Wang G, and Zhou X 2022 *Advanced Functional Materials* **32** 2206974
[43] Yang X, Liu Z, Meng F, and Li W 2021 *Phys. Rev. B* **104** L100306
[44] Kundu A, Yang X, Ma J, Feng T, Carrete J, Ruan X, Madsen G K H, and Li W 2021 *Phys. Rev. Lett.* **126** 115901
[45] Quan Y, Yue S, and Liao B 2021 *Nanoscale and Microscale Thermophysical Engineering* **25** 73
[46] Emmanouilidou E, Mardanya S, Xing J, Reddy P V S *et al.* 2020 *Phys. Rev. B* **102** 235144
[47] Remeika J P, Cooper A S, Fisk Z, and Johnston D C 1978 *Journal of the Less Common Metals* **62** 211
[48] Brixner L H 1963 *Journal of Inorganic and Nuclear Chemistry* **25** 257
[49] Gottlieb U, Laborde O, Thomas O, Rouault A, Senateur J P, and Madar R 1991 *Applied Surface Science* **53** 247